Numerical Analyses on the Reflection of Ionizing Shocks on an End Wall of a Shock Tube

By

Yasunari TAKANO* and Teruaki AKAMATSU*

(Rceived January 25, 1977)

Abstract

Numerical analyses have been made on the ionizing shock reflection on a closed end of a shock tube by the use of the finite difference method. It was found that very interesting phenomena and complicated flowfields occur due to the interaction between inoization relaxation and reflected shocks. The exact numerical solutions were compared with the results of some simplified models. Calculations were performed for argon.

Nomenclature

a: speed of sound

c: degree of ionization

$\dot{c}$: net degree of ionization production rate

$\dot{c}_e$: net degree of ionization production rate due to electron-atom inelastic collisions

c_{eq}: equilibrium reference degree of ionization

C: Courant number

e: energy, electric charge

E_I: ionization energy

k: Boltzmann constant

k_{ra}, k_{re}: ionization rate constants

m_e: mass of an electron

m_h: mass of a heavy particle

n_e: number density of electron gas

$\dot{n}_e$: net rate of electron production

$(\dot{n}_e)_e$: net rate of electron production due to electron-atom inelastic collisions

p: pressure

R: gas constant

t: time after shock reflection

* Department of Mechanical Engineering

T: temperature of heavy particle gas
T_e: temperature of electron gas
T_{A1}: characteristic temperature of excitation
$T_{ion}(=E_I/k)$: characteristic temperature of ionization
u: velocity
u_S: speed of incident shock
u_R: speed of reflected shock
u_{RF}, u_{RFE}, u_{RE}: speeds of reflected shocks in simplified models
x: distance from shock tube end wall
ν_{eh}: collision frequency for electron-heavy particle
ρ: density

Subscripts

j: grid point of x-coordinate
n: grid point of t-coordinate
1: initial region (Fig. 1)

1. Introduction

High-temperature stagnant gases and plasmas can be generated behind shock waves reflected from a closed end of a shock tube. These hot gas regions are used to study the ionization relaxation[1,2] and the thermal boundary layer.[3,4] Therefore, it is important to realize the situation in the flowfield behind the reflected shock. Several experimental investigations[1,5,6] have indicated that interactions between the reflected shocks and the ionization relaxation processes make flowfields very complex. Some explanations[1,5] have been made about such phenomena, but there do not seem to be any detailed elucidations.

The purpose of the present paper is to investigate, in more detail, the situation by numerical analyses with the use of the finite difference method. The present problem is concerned with the flowfields where ionizing shock waves reflect from the end wall of a shock tube and propagate back into the ionizing nonequilibrium argon gases, which incident shocks have left behind. Moreover, we assume some simplified models to get approximate estimations about flowfields behind the reflected shocks, and then compare them with the exact numerical results.

2. Analysis

A schematic distance-time diagram is shown in Fig. 1, where x is the distance from the shock-tube end-wall and t is the time elapsed after the reflection

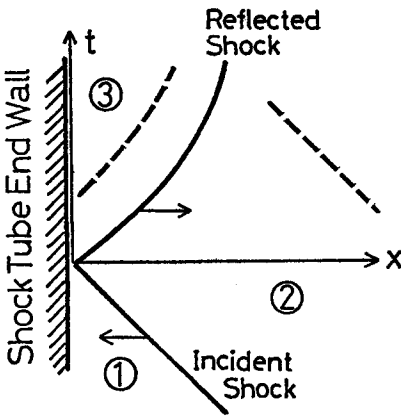

Fig. 1. Schematic distance and time diagram for shock reflection on the end wall.

of a shock. The problem to be solved is an initial value problem with some boundary conditions at the shock tube end.

2.1 Basic equations

The basic equations used here are unsteady one-dimensional conservation equations for ionized and thermally nonequilibrium inviscid gases

$$\frac{\partial \rho}{\partial t}+\frac{\partial(\rho u)}{\partial x}=0 \tag{1}$$

$$\frac{\partial(\rho u)}{\partial t}+\frac{\partial(\rho u^2+p)}{\partial x}=0 \tag{2}$$

$$\frac{\partial}{\partial t}\left[\rho\left(e+\frac{u^2}{2}\right)\right]+\frac{\partial}{\partial x}\left[\rho u\left(e+\frac{u^2}{2}+\frac{p}{\rho}\right)\right]=0 \tag{3}$$

and equations of state for monatomic gases.

$$p=\rho R(T+cT_e) \tag{4}$$

$$e=\frac{3}{2}\frac{p}{\rho}+cRT_{ion} \tag{5}$$

Next, conservation equations of mass and energy of the electron gas[7,8] are

$$\frac{\partial n_e}{\partial t}+\frac{\partial(n_e u)}{\partial x}=\dot{n}_e \tag{6}$$

$$\frac{\partial}{\partial t}\left(\frac{3}{2}n_e kT_e\right)+\frac{\partial}{\partial x}\left(\frac{3}{2}n_e kT_e u\right)+n_e kT_e\frac{\partial u}{\partial x}$$

$$=3\frac{m_e}{m_h}n_e k(T-T_e)\nu_{eh}-E_I(\dot{n}_e)_e \tag{7}$$

The following equation can be written in terms of the degree of ionization

$$\frac{\partial(\rho c)}{\partial t}+\frac{\partial(\rho c u)}{\partial x}=\rho \dot{c} \tag{8}$$

where $\dot{c}$ is the degree of ionization production rate, which will be described in the next section. The electron gas is assumed to be in a local steady state: each term on the left hand side of Eq. (7) is much smaller than either of the terms on the right hand side. Thus, the following equation[8] is used instead of Eq. (7).

$$T-T_e=\frac{1}{3}\frac{\dot{c}_e/c}{(m_e/m_h)\nu_{eh}}T_{ion} \tag{9}$$

The local steady state approximation is known to be valid in almost all the parts of the relaxation zone, except the initial stage of the ionization relaxation immediately behind an incident shock.

The above-mentioned differential equations are to be solved with the following initial and boundary conditions. Concerning the boundary conditions at $x=0$, we assume that the surface of the shock-tube end-wall is impermeable and thermally insulated. This means that two shock waves with equal strength collide with each other at the symmetric plane ($x=0$). The initial conditions are given by the profiles of the ionization relaxation behind the incident shock propagating into the stationary region. The scheme determining these profiles is given in the Appendix.

2.2 Ionization production rates and collision frequencies

The net degree of the ionization production rate[8] $\dot{c}$ consists of two processes. One is the production due to atom-atom inelastic collisions

$$\dot{c}_a=(1-c)\left(\frac{\rho}{m_h}\right)^2 k_{ra}(T)\left[\frac{c_{eq}^2(T)-c^2}{1-c_{eq}^2(T)}\right] \tag{10}$$

The other is the production due to electron-atom collisions

$$\dot{c}_e=c\left(\frac{\rho}{m_h}\right)^2 k_{re}(T_e)\left[\frac{c_{eq}^2(T_e)-c^2}{1-c_{eq}^2(T_e)}\right] \tag{11}$$

Therefore, the net rate is written as follows

$$\dot{c}=\dot{c}_a+\dot{c}_e \tag{12}$$

$c_{eq}(T)$ and $c_{eq}(T_e)$ in Eqs. (10) and (11) are the equilibrium reference degrees of ionization which are written as

$$c_{eq}(T_M) = \left[1+\frac{\rho(1+c)}{m_h K_{eq}(T_M)}\right]^{-1/2} \tag{13}$$

where $K_{eq}(T_M)$ is the equilibrium constant ($T_M = T$ or T_e)

$$K_{eq}(T_M) = \frac{2Z_i}{Z_a}\left(\frac{2\pi m_e k T_M}{h^2}\right)^{3/2}\exp\left(-\frac{T_{ion}}{T_M}\right) \tag{14}$$

Z_a and Z_i in Eq. (14) are the electronic partition functions of atoms and ions, and their ratio for argon can be approximated by $Z_i/Z_a=6$. The rate constants of argon used in the numerical analysis are

$$k_{ra}(T) = 5.80\times10^{-37}\left(\frac{T_{A1}}{T}+2\right)\exp\left(\frac{T_{ion}-T_{A1}}{T}\right) \quad \frac{\text{cm}^6}{\text{s}} \tag{15}$$

$$k_{re}(T_e) = 1.29\times10^{-32}\left(\frac{T_{A1}}{T_e}+2\right)\exp\left(\frac{T_{ion}-T_{A1}}{T_e}\right) \quad \frac{\text{cm}^6}{\text{s}} \tag{16}$$

where $T_{ion}=183100°\text{K}$ and $T_{A1}=135300°\text{K}$.

The elastic collision frequency[8] between electrons and heavy particles ν_{eh} is the sum of electron-ion collision frequency ν_{ei} and electron-atom collision frequency ν_{ea}.

$$\nu_{eh} = \nu_{ei}+\nu_{ea} \tag{17}$$

$$\nu_{ei} = \frac{c\rho}{m_h}\left(\frac{8kT_e}{\pi m_e}\right)^{1/2}Q_{ei} \tag{18}$$

$$\nu_{ea} = \frac{(1-c)\rho}{m_h}\left(\frac{8kT_e}{\pi m_e}\right)^{1/2}Q_{ea} \tag{19}$$

The elastic collision cross section between electrons and atoms[9] adopted in the present numerical calculations is

$$\begin{aligned} Q_{ea} &= (-0.35+0.775\times10^{-4}T_e)\times10^{-16}\,cm^2, \quad 10^{4°}\text{K}<T_e<5\times10^{4°}\text{K} \\ &= (0.39-0.551\times10^{-4}T_e+0.595\times10^{-8}T_e^2)\times10^{-16}\,cm^2, \quad T_e<10^{4°}\text{K} \end{aligned} \tag{20}$$

and the elastic collision cross section for electrons and ions[9] can be expressed as

$$Q_{ei} = \frac{2\pi e^4}{9k^2T_e^2}\ln\left(\frac{9k^3T_e^3}{4\pi e^6 n_e}\right) \tag{21}$$

3. Finite difference method

3.1 Finite difference equations

On writing

$$\rho' = \frac{\rho}{\rho_1}, \quad u' = \frac{u}{u_S}, \quad e' = \frac{e}{u_S^2}$$

$$p' = \frac{p}{\rho_1 u_S^2}, \quad t' = \frac{t}{\tau}, \quad x' = \frac{x}{\tau u_S} \tag{22}$$

and dismissing primes, the basic equations are reduced to

$$\frac{\partial U}{\partial t} + \frac{\partial F}{\partial x} = G \tag{23}$$

$$U = \begin{pmatrix} \rho \\ \rho u \\ \rho\left(e + \frac{u^2}{2}\right) \\ \rho c \end{pmatrix}, \quad F = \begin{pmatrix} \rho u \\ \rho u^2 + p \\ \rho u\left(e + \frac{u^2}{2} + \frac{p}{\rho}\right) \\ \rho c u \end{pmatrix}, \quad G = \begin{pmatrix} 0 \\ 0 \\ 0 \\ \tau \rho \dot{c} \end{pmatrix} \tag{24}$$

where τ is the characteristic time of the ionization relaxation[5] which is written as

$$p_1 \tau = 0.156 \exp\left(87000°\mathrm{K}/T_{2F}\right) \qquad \text{torr} \cdot \mu s \tag{25}$$

and T_{2F} is the frozen temperature just behind an incident shock.

The finite difference method used in the present numerical analysis is the two-step Lax-Wendroff scheme[10], shown as follows:

$$U_j^{n+1} = U_j^n - \frac{\lambda}{2}\left\{\frac{1}{2}\left(F_{j+1}^n - F_{j-1}^n\right) + \left(\tilde{F}_{j+(1/2)}^{n+1} - \tilde{F}_{j-(1/2)}^{n+1}\right)\right\} + G_j^{n+(1/2)} \Delta t \tag{26}$$

$$G_j^{n+(1/2)} = G\left[\frac{1}{4}\left(2U_j^n + \tilde{U}_{j+(1/2)}^{n+1} + \tilde{U}_{j-(1/2)}^{n+1}\right)\right]$$

$$\tilde{F}_{j+(1/2)}^{n+1} = F\left[\tilde{U}_{j+(1/2)}^{n+1}\right] \tag{27}$$

$$\tilde{U}_{j+(1/2)}^{n+1} = \frac{1}{2}\left(U_{j+1}^n + U_j^n\right) - \lambda\left(F_{j+1}^n - F_j^n\right) + G_{j+(1/2)}^n \Delta t$$

$$G_{j+(1/2)}^n = G\left[\frac{1}{2}\left(U_{j+1}^n + U_j^n\right)\right] \tag{28}$$

where subscripts j and n refer to the grid points of the x and t coordinates, Δx and Δt are stepsizes of them and $\lambda = \Delta t/\Delta x$, which must satisfy the Courant-Friedrich-Lewy condition,

$$\frac{\Delta t}{\Delta x} = C \frac{1}{\mathrm{Max}(a + |u|)} \tag{29}$$

$$0 < C < 1 \tag{30}$$

where a is the speed of sound given by

$$a^2 = \frac{5}{3}\frac{p}{\rho} \tag{31}$$

and C is the Courant number.

3.2 Boundary Conditions and Initial Conditions

In the previous section, the conditions of symmetricity have been shown to hold at the shock tube end wall ($x=0$). These conditions are made use of in the present finite difference scheme. The grid point $j=0$ is located at $x=0$. U^n_{-1}at the grid point $j=-1$ is determined in such a way that

$$u^n_{-1} = -u^n_1 \tag{32}$$

$$\rho^n_{-1} = \rho^n_1, \quad p^n_{-1} = p^n_1, \quad e^n_{-1} = e^n_1, \quad c^n_{-1} = c^n_1 \tag{33}$$

If $U^n_j (j=0, \cdots, N)$ is known, U^n_{-1} is given by Eqs. (32) and (33), and then $U^{n+1}_j (j=0, \cdots, N-1)$ is evaluated by Eq. (26). When U^n_j is in the equilibrium state behind the incident shock, U^{n+1}_j can be determined by the relation $U^{n+1}_j = U^n_j$. Initial data at the grid points are given by the ionization relaxation profiles (Appendix).

It takes a very long time to begin the difference scheme with the above-mentioned initial data which consist of three main regions: a cold stationary region in front of a shock, a frozen hot region and an equilibrium region behind a shock. Therefore, we start the difference scheme within a smaller domain, shown in Fig. 2. The computation domain spreads zigzagingly according to the propagation of the reflected shock. The zigzag boundary conditions are evaluated by the relation

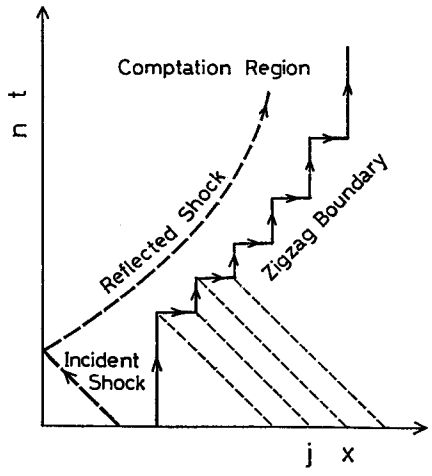

Fig. 2. Schematic diagram of the computation region for the shock reflection problem.

$U(x, t+\xi)=U(x+\xi, t)$. Considering that the normalized velocity of the incident shock is unity, the above-mentioned relation is valid for the region behind the incident shock.

4. Results of Numerical Calculations

Numerical calculations have been obtained on Kyoto University's Computor FACOM 230–75 for three cases, shown in Table 1, which are experimentally achieved by our shock tube facilities. The Courant number defined in Eq. (29), is 0.9

Table 1. Conditions of numerical analyses: Incident shock Mach numbers, initial pressure and step sizes of finite difference scheme.

Case	Ms	p_1 (torr.)	Δx	Δt
1	16	1	0.005	0.0034374
2	14	3	0.004	0.0027426
3	12	5	0.002	0.0013659

for each case. The $x-t$ diagrams of these three cases are shown in Figs. 3,4 and 5, where n indicates the number of computation steps. Figure 6 shows the profiles of T, u, T_e, ρ, p and c behind the incident shock of Case 1. With reference to Fig 3, let us explain the flowfields across the reflected shocks. For a short time after the reflection of the incident shock, the region between the end wall and the reflected shock is in a frozen state ($n=40\sim100$). Then, the ionization relaxation proceeds in the nonequilibrium region, and the reflected shock begins to move rather slowly ($n=100\sim150$). Meanwhile, with ionization suddenly occurring, the gases in the nonequilibrium region turn out into an equilibrium state initiated at the end wall ($n=200$). In this equilibrium region adjacent to the end wall, the temperature goes down and the density increases because the ionization reaction removes the ionization energy from the kinetic energy in gases. Therefore, an expansion wave propagates from the equilibrium region adjacent to the end wall, which weakens the reflected shock in velocity ($n=300\sim500$). Figure 7 shows the flowfield of Case 1 at $n=300$. The reflected shock is seen at $x=0.41$ and the gases upstream of it are in a nonequilibrium state. In the neighborhood of the reflected shock, some vibrations are seen which often appear in results of the finite difference scheme. The gas near the end wall ($0\leq x\lesssim0.5$) attains an equilibrium state and the expansion wave is seen which has the minimum of pressure at $x=0.19$. As gases in front of the reflected shock relax into an equilibrium state, the reflected shock slows down in velocity and at last goes back towards the end wall ($n=500\sim700$, Fig. 3). This phenomenon is caused by the fact that the increase in the density

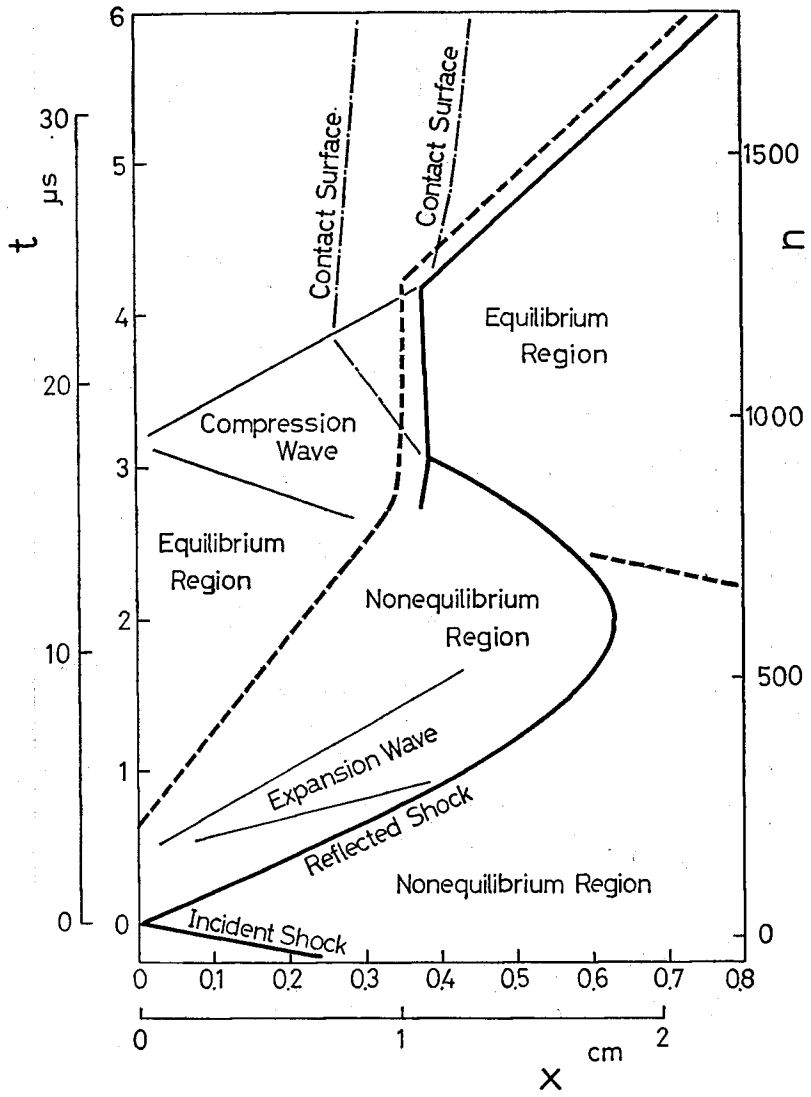

Fig. 3. $x-t$ diagram of the shock reflection process obtained by the numerical analysis of the case 1; Ms=16 and $p_1=1$ torr.

in front of the reflected shock weakens the reflected shock in strength. The reflected shock, propagating back to the end wall, interacts with the equilibrium region behind it. The typical profiles of the flowfields marked with ①, ②, ③, and ④ in Fig. 4 are shown in Fig. 8. The reflected shock is denoted by 1R, 2R, etc and the onset of the equilibrium region is denoted by 1E, 2E, etc. Profile 1 shows the flowfield where the reflected shock almost ceases moving, and its gas upstream is still in a nonequilibrium state. In profile 2, the retiring shock decreases in

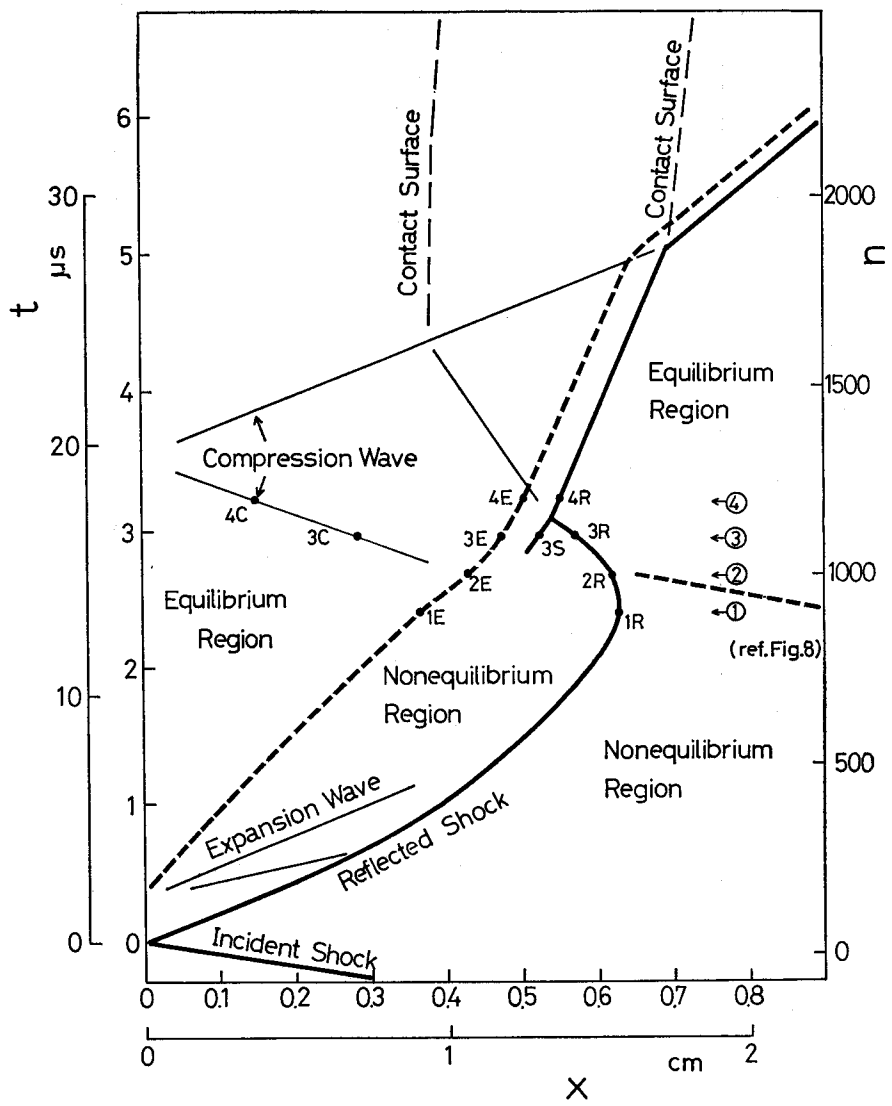

Fig. 4. $x-t$ diagram of the shock reflection process obtained by the numerical analysis of the case 2; Ms=14 and p_1=3 torr.

strength, whereby the pressure and the temperature of the nonequilibrium region behind it become low. However, the pressure in the neighborhood of point 2E grows high, and the temperature of the relaxation region becomes higher at the last stage of relaxation because of the gas moving against the steep pressure gradient. In profile 3, from the high-pressure zone (3E) between the equilibrium region and the nonequilibrium region, a compression wave (3C) is generated, propagating to

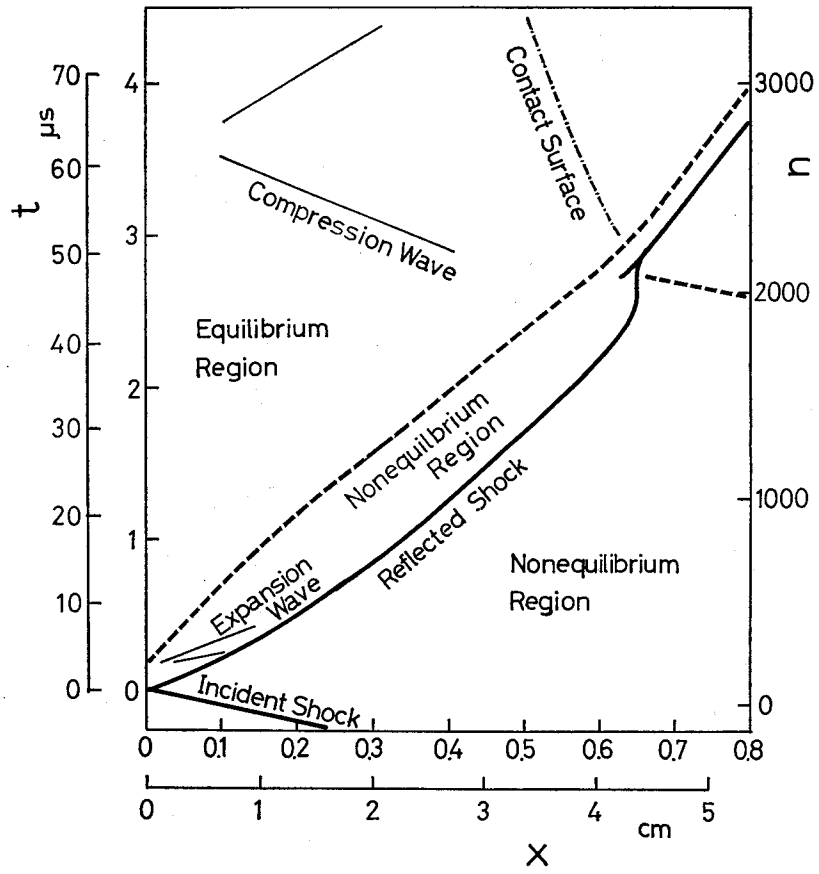

Fig. 5. $x-t$ diagram of the shock reflection process obtained by the numerical analysis of the case 3; Ms=12 and p_1=5 torr.

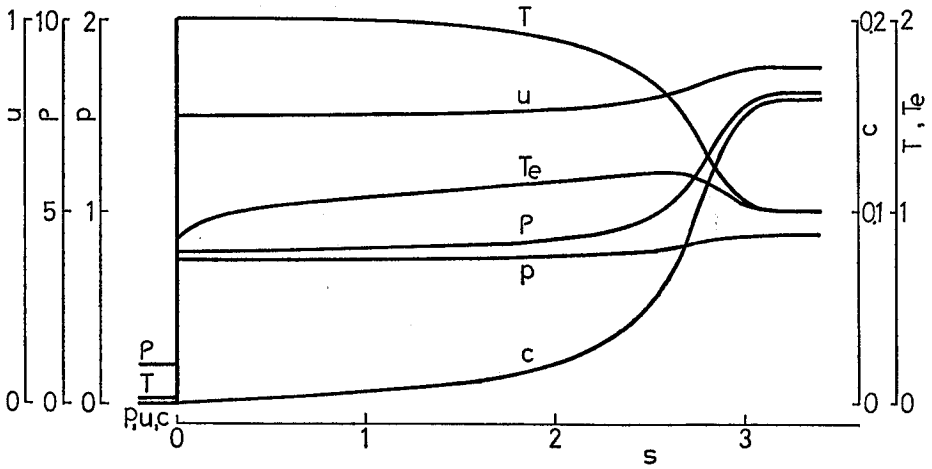

Fig. 6. Flowfield behind the incident shock used for initial data of the numerical analysis of the case 1.

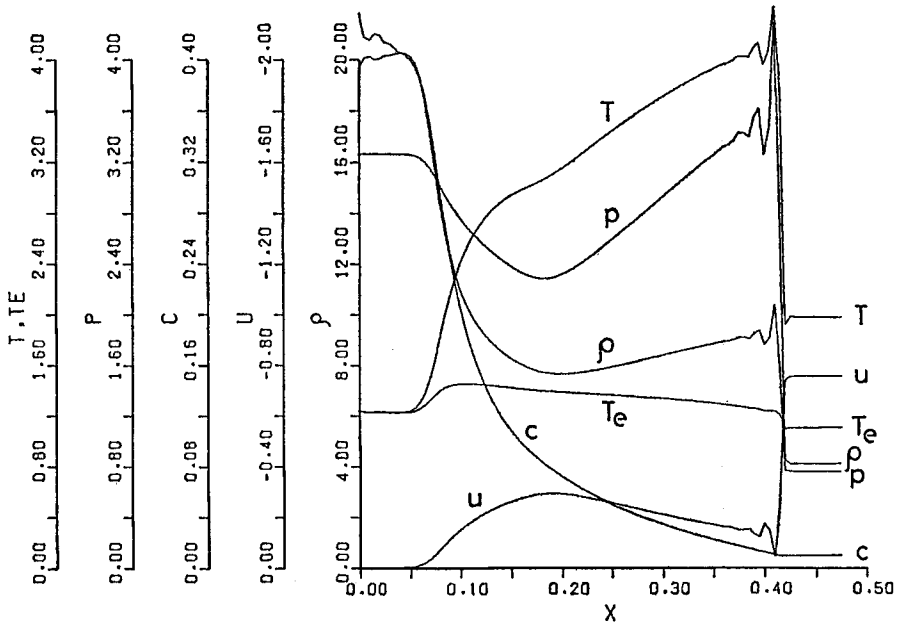

Fig. 7. Flowfield behind the reflected shock for the case 1 obtained by the numerical analysis at $n=300$.

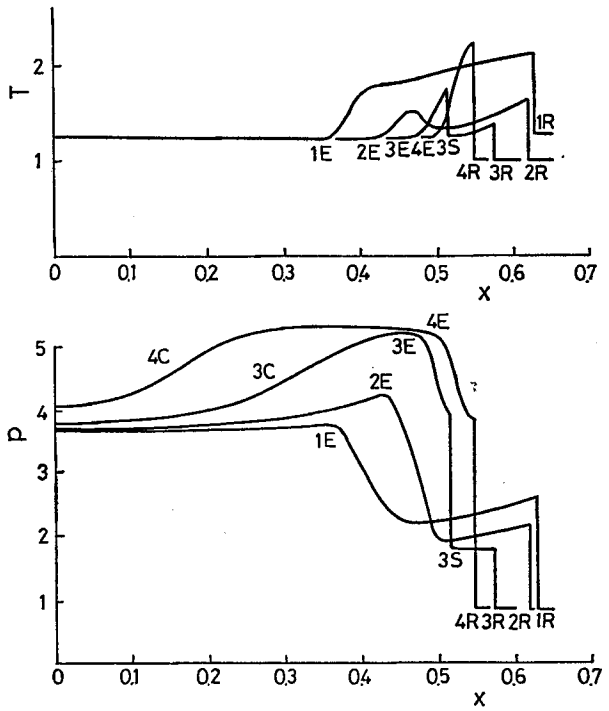

Fig. 8. Flowfields behind the reflected shock for the case 2 with the mark; Numbers 1, 2, 3 and 4 refer to computation steps $n=900$, $n=1000$ $n=1100$ and $n=1200$ respectively and R, S, E and C mean reflected shock, newly generated shock, onset of equilibration and compression wave respectively.

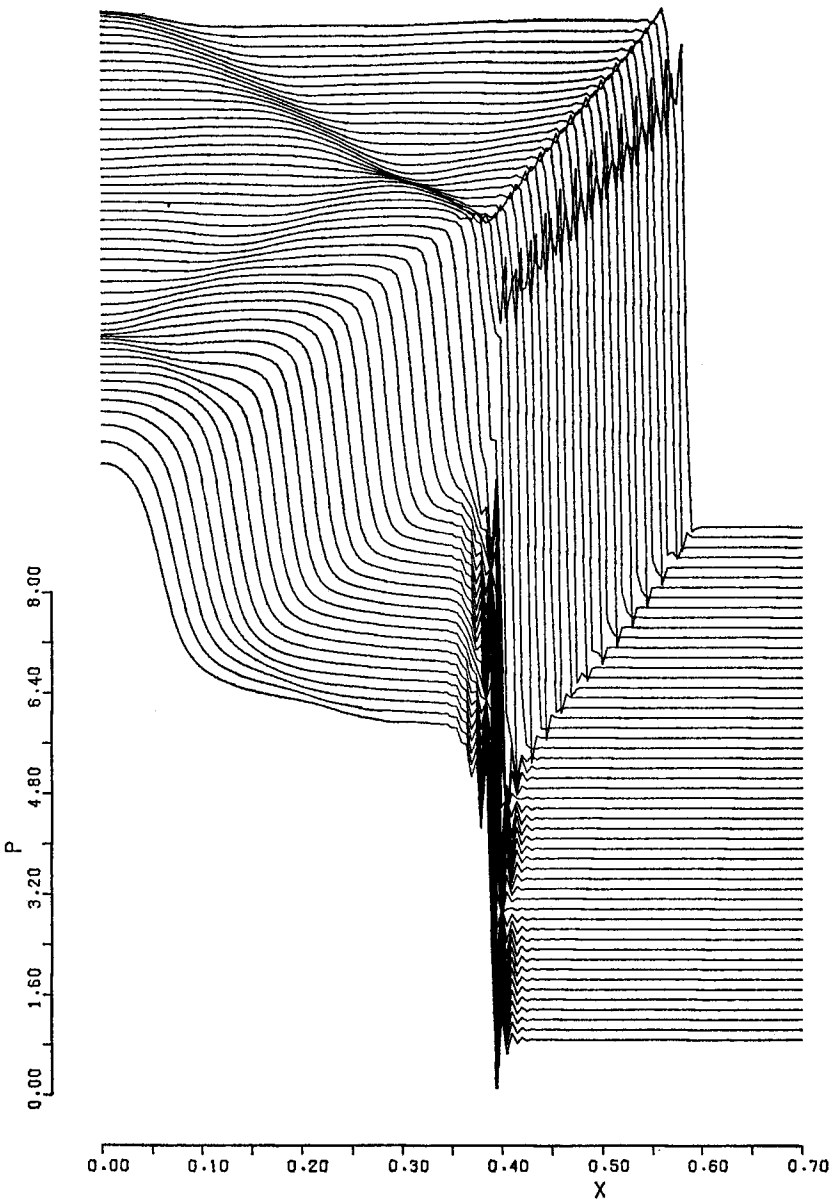

Fig. 9. Variations of the pressure profile behind the reflected shock for case 1 at every 10 computation steps from $n=990$ to $n=1500$.

the end wall. Simultaneously, a shock (3S) is also produced moving to the reflected shock. The colliding of this newly generated shock with the reflected shock gives rise to a contact surface where the density and the degree of ionization are discontinuous but the temperature is almost continuous. Figures 9 and 10

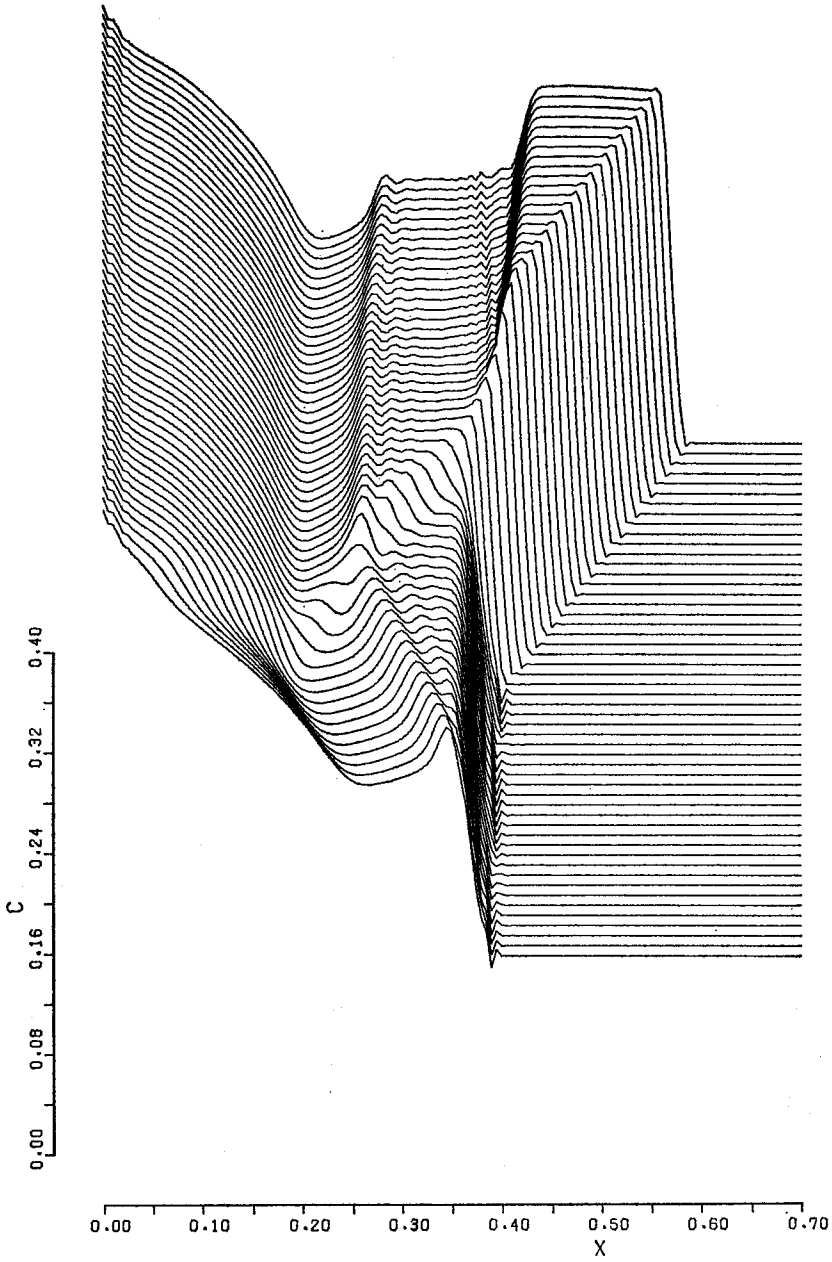

Fig. 10. Variations of the degree of ionization profile behind the reflected shock for case 1 at every 10 computation steps from $n=990$ to $n=1500$.

show 52 profiles of the pressure and the degree of ionization of Case 1 (Fig. 3) plotted one above another with the values shifting from $n=990$ to $n=1500$ at every 10 computation steps. The compression wave moving to the end wall

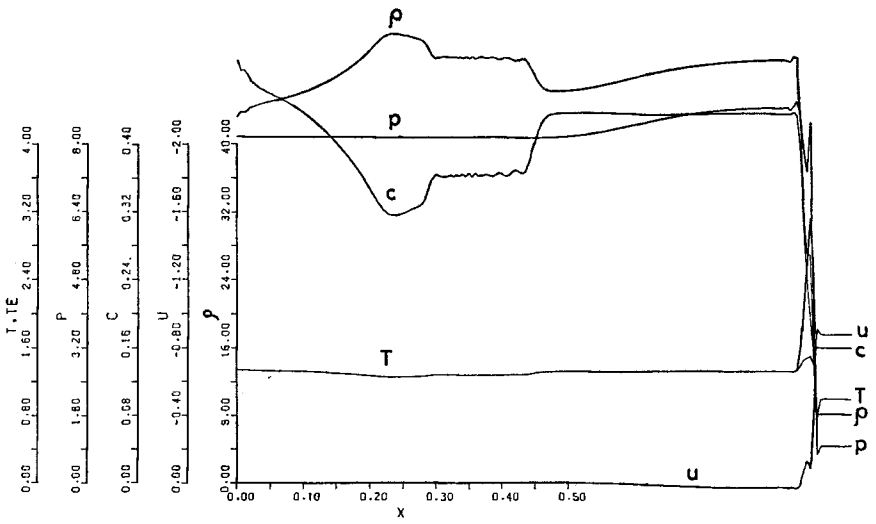

Fig. 11. Flowfield behind the reflected shock for case 1 at $n=1900$.

($n=800\sim950$), reflects there, catches up with the reflected shock and strengthens it ($n=1260$). There is also generated another contact surface where the density and the degree of ionization are again discontinuous but the temperature is almost continuous. Figure 11 shows the profiles of the hot stagnant region where the reflected shock passed through ($n=1900$). The pressure and temperature profiles are uniform there, but the profiles of the density and the degree of ionization are complicated due to interactions between the ionization relaxation phenomena and waves.

5. Comparison with some simplified models

Some methods to estimate the actual states in the regions behind the reflected shocks are necessary for experimental investigation. Therefore, we estimate them by simplified models and compare them with the numerical exact solutions. As shown in the present numerical analyses, the region behind the incident or the reflected shock is not straightforward. However, simplifications are made so that the region behind the incident shock or the reflected shock is uniform and is in a frozen or equilibrium state. The following simplified models are treated as shown in Fig. 12:

(1) The frozen incident shock reflects on the end wall and propagates back into the frozen region (2F) with the frozen velocity of u_{RF}. These conditions are realized in the shock reflection of perfect gases, or immediately behind the reflected shock of real gases.

(2) The reflected shock moves into the frozen region (2F) with the ideal velocity of u_{RFE}, while the whole region behind the reflected shock is assumed to be in an equilibrium state.

(3) The equilibrium incident shock reflects at the end wall and propagates back into the equilibrium region (2E) with the equilibrium velocity of u_{RE}. Namely, the regions in front of and behind the reflected shock are both in an equilibrium state.

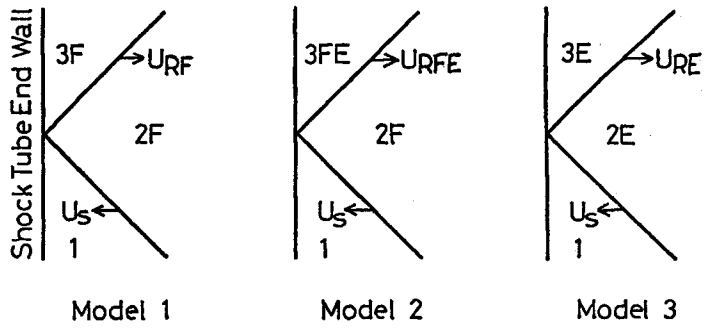

Fig. 12. Schematic diagarm for simplified models.

Table 2. Conditions of flowfield obtained by the simplified models shown in Fig. 12 schematically. (T_1=300°K)

Case	Ms	p_1 (torr.)	ρ_1 (g/cm^3)	ρ_{2F}/ρ_1	ρ_{2E}/ρ_1	ρ_{3F}/ρ_1	ρ_{3FE}/ρ_1
1	16	1	2.13×10^{-6}	3.95	8.15	9.84	22.8
2	14	3	6.40×10^{-6}	3.94	6.53	9.79	19.4
3	12	5	1.07×10^{-6}	3.92	5.21	9.71	16.5

Case	ρ_{3E}/ρ_1	T_{2E} (°K)	T_{2F}/T_{2E}	T_{3F}/T_{2E}	T_{3FE}/T_{2E}	T_{3E}/T_{2E}
1	48.4	11913	2.04	4.85	1.20	1.32
2	33.3	11690	1.59	3.79	1.21	1.32
3	22.6	10798	1.27	3.01	1.21	1.32

Case	c_{2E}	c_{3FE}	c_{3E}	u_S (Km/s)	u_{2F}/u_S	u_{2E}/u_S	u_{RF}/u_S
1	0.160	0.346	0.422	5.16	0.747	0.877	−0.502
2	0.0913	0.238	0.283	4.52	0.746	0.847	−0.503
3	0.0401	0.150	0.171	3.87	0.745	0.808	−0.503

Case	u_{RFE}/u_S	u_{RE}/u_S
1	−0.157	−0.178
2	−0.190	−0.207
3	−0.232	−0.242

Table 2 shows the gas quantities for the three cases obtained by the simplified models. Some comparisons between the simplified models and the numerical analyses will be made. In the region behind the reflected shock where the rapid ionization reaction has not yet occurred, the gas quantities are nearly equal to the data of the 3F region. After a while, this gas ionizes and then becomes an equilibrium state. The pressure and the temperature are nearly equal to those of the 3FE region respectively, but the density is lower and the degree of ionization is higher than those of the 3FE region. Processes of the ionization relaxation and the interaction of waves occur, and finally a hot stagnant equilibrium gas is produced. The pressure and the temperature of this region are nearly equal to the data of the 3E region, but the profiles of the density and the degree of ionization shown in Fig. 11 are too complicated to compare with the data of the simplified models.

In the above-mentioned simplified models 2 and 3, the gases behind the reflected shock are assumed to be in a uniformly equilibrium state, even immediately behind the reflected shock. Also, the ionization relaxation behind the reflected shock is neglected and the flowfield is over-simplified. Then, taking into account the ionization relaxation behind the reflected shock, let us deal with the following two modified models shown in Fig. 13; (a) the reflected shock with the constant

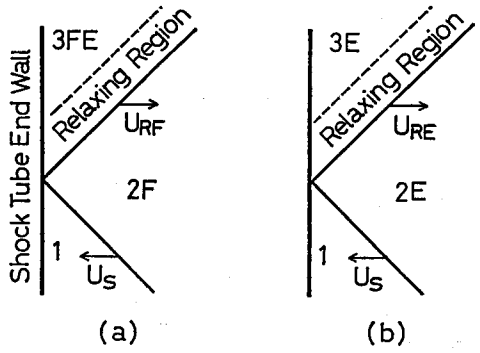

Fig. 13. Schematic diagram for modified reflected shock.

velocity of u_{RFE} moves into the 2F region; (b) the reflected shock with the constant velocity of u_{RE} moves into the 2E region. The profiles of the ionization relaxation behind the reflected shocks can be determined by the procedures given in the Appendix. When $t>4$ in Fig. 3, the velocity of the reflected shock does not seem to change, and the gas in front of this reflected shock is in an equilibrium state. Hence, it may be worth while to compare the profiles of the ionization relaxation behind the reflected shock specified with the velocity of u_{RE} (Model *b*) with the exact numerical results of Case 1. Figure 14 shows that there is a good agreement between

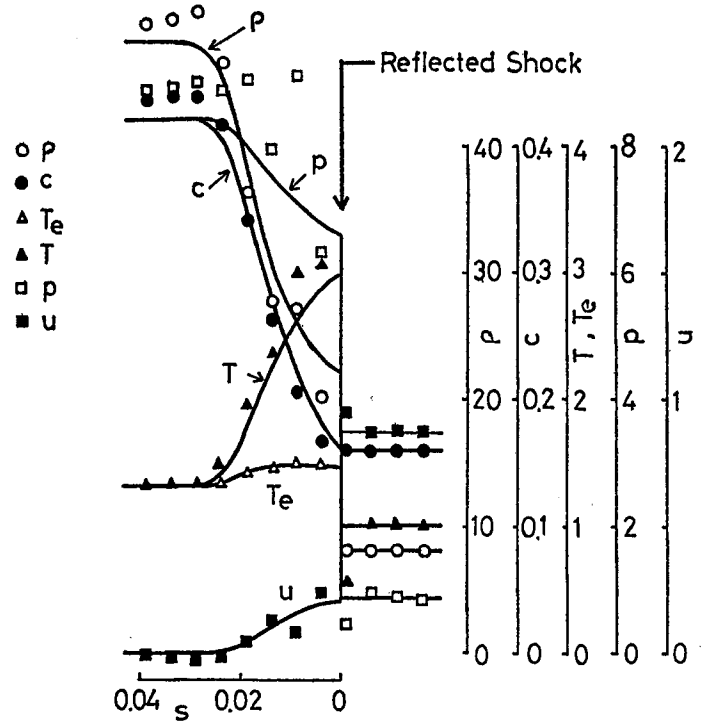

Fig. 14. Flowfield behind modified reflected shock for the case 1 (solid lines) and comparison with the results of numerica analysis (marks).

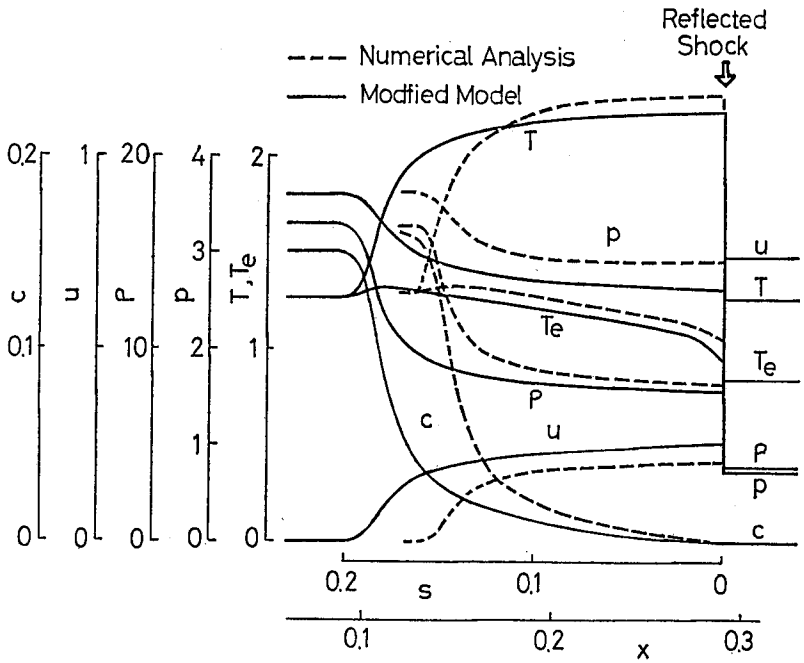

Fig. 15. Comparisons of flowfields with modified model (solid lines) and numerical analysis (broken lines).

the results by the modified model and the exact numerical results at $n=1980$, except for some vibrations inherent to the finite difference schemes. When $0.5<t<1$ in Case 3, the velocity u_R, as shown in Fig. 5, varies extremely slowly and the gas in front of the reflected shock seems to be in a frozen state. The profiles for the modified model *a* are shown in Fig. 15. The relaxation distance of the exact numerical result at $n=700$ ($t=0.856$) is shorter than that of the modified model by 25 %. This shortening is because the gas upstream of the reflected shock is not really in a frozen state, but already has some degree of ionization of about 0.1 % at $n=700$.

6. Conclusion

Numerical analyses about the ionizing shock reflection on a closed end of a shock tube have been performed with the use of the finite difference method. Some interesting phenomena and complicated flowfields have been found, which occur due to the interaction between ionization relaxation and reflected shocks. While several explanations have been made about the exact numerical analyses. The effects of the radiation energy loss have been neglected in this study. However, the present finite difference procedure may be applied to solve such problems, including the radiation effect.

Appendix

The flow across a normal standing shock is governed by the following equations[8]

$$\rho u = \rho_0 u_0 \tag{A1}$$

$$p+\rho u^2 = p_0+\rho_0 u_0^2 \tag{A2}$$

$$h+\frac{1}{2}u^2 = h_0+\frac{1}{2}u_0^2 \tag{A3}$$

$$p = \rho R(T+cT_e)\,, \quad p_0 = \rho_0 R(1+c_0)\,T_0 \tag{A4}$$

$$h = \frac{5}{2}\frac{p}{\rho}+cRT_{ion}\,, \quad h_0 = \frac{5}{2}\frac{p_0}{\rho_0}+c_0RT_{ion} \tag{A5}$$

where the subscript 0 refers to upstream conditions. These equations are derived to the following relations:

$$\frac{u_0}{u} = \frac{1}{4}\left\{\frac{5}{2}\left(1+\frac{p_0}{\rho_0 u_0^2}\right)-\sqrt{\left(\frac{3}{2}-\frac{5}{2}\frac{p_0}{\rho_0 u_0^2}\right)^2+8(c-c_0)\frac{RT_{ion}}{u_0^2}}\right\} \tag{A6}$$

$$\frac{p}{p_0} = 1+\frac{\rho_0 u_0^2}{p_0}\left(1-\frac{u}{u_0}\right) \tag{A7}$$

$$\frac{\rho}{\rho_0} = \frac{u_0}{u} \tag{A8}$$

The degree of ionization is determined by the rate equation

$$\frac{dc}{ds} = \frac{\dot{c}_a + \dot{c}_e}{u} \tag{A9}$$

where the coordinate s is the distance from the shock front. The temperature of electron gas is assumed to be given by Eq. (9). The initial condition for Eq. (A9) is $c=c_0$ at $s=0$, which is the degree of ionization immediately behind the shock. Therefore, the ionization relaxations behind the incident shock are represented as functions of the distance s measured from the travelling shock. Incorporating Eqs. (A6)$\sim$(A8) substituted with the upstream conditions of $u_0=u_S$, $\rho_0=\rho_1$, $p_0=p_1$, $h_0=h_1$ and $c_0=c_1=0$, the differential equation (A9) can be solved by using the Runge-Kutta-Gill method with the initial condition of $c=0$.

The flow behind the reflected shock specified with a constant velocity and constant upstream conditions can be also similarly determined. The upstream conditions for the model (a) are $u_0=u_{2F}-u_{RFE}$, $\rho_0=\rho_{2F}$, $p_0=p_{2F}$, $h_0=h_{2F}$ and $c_0=c_{2F}=0$, and the initial condition for Eq. (A9) is $c=0$. For the model (b), the upstream conditions are $u_0=u_{2E}-u_{RE}$, $\rho_0=\rho_{2E}$, $p_0=p_{2E}$, $h_0=h_{2E}$ and $c_0=c_{2E}$, and the initial condition is $c=c_{2E}$, which is the degree of ionization immediately behind the reflected shock front.

References

1) J.A. Smith, Phys. Fluids, **11**, 2150 (1968).
2) K. Fukuda, I. Sugiyama and R. Okasaka, J. Phys. Soc. Japan, **35**, 1202 (1973).
3) J.A. Fay and N.H. Kemp, J. Fluid Mech. **21 4**, 659 (1965).
4) M. Camac and R.M. Feinberg J. Fluid Mech. **21 4**, 673 (1965).
5) H.S. Friedman and J.A. Fay, Phys. Fluids, **8**, 1968 (1965).
6) R.A. Kuiper, Proc. 7th Int. Shock Tube Sym. Canada, 721 (1969).
7) G.W. Sutton and A. Sherman, Engineering Magnetohydrodynamics, McGraw-Hill, Inc. New York (1965).
8) Hoffert and Lien, Phys, Fluids, **10**, 1769 (1967).
9) M.Y. Jaffrin, Phys. Fluids, **8**, 606 (1965).
10) E.L. Rubin and S.Z. Burstein, J. Comp. Phys., **2**, 178 (1967).